Accepted Manuscript

Synthesis of gold(I) phosphine complexes containing the 2-$BrC_6F_4PPh_2$ ligand: Evaluation of anticancer activity in 2D and 3D spheroidal models of HeLa cancer cells

T. Srinivasa Reddy, Steven H. Privér, Nedaossadat Mirzadeh, Suresh K. Bhargava

PII: S0223-5234(17)31080-2

DOI: 10.1016/j.ejmech.2017.12.048

Reference: EJMECH 10026

To appear in: *European Journal of Medicinal Chemistry*

Received Date: 3 November 2017

Revised Date: 12 December 2017

Accepted Date: 13 December 2017

Please cite this article as: T.S. Reddy, S.H. Privér, N. Mirzadeh, S.K. Bhargava, Synthesis of gold(I) phosphine complexes containing the 2-$BrC_6F_4PPh_2$ ligand: Evaluation of anticancer activity in 2D and 3D spheroidal models of HeLa cancer cells, *European Journal of Medicinal Chemistry* (2018), doi: 10.1016/j.ejmech.2017.12.048.

Synthesis of gold(I) phosphine complexes containing the 2-$BrC_6F_4PPh_2$ ligand: Evaluation of anticancer activity in 2D and 3D spheroidal models of HeLa cancer cells

T. Srinivasa Reddy, Steven. H. Privér, Nedaossadat. Mirzadeh,* Suresh. K. Bhargava*

Centre for Advanced Materials & Industrial Chemistry (CAMIC), School of Science, RMIT University, GPO BOX 2476, Melbourne 3001, Australia

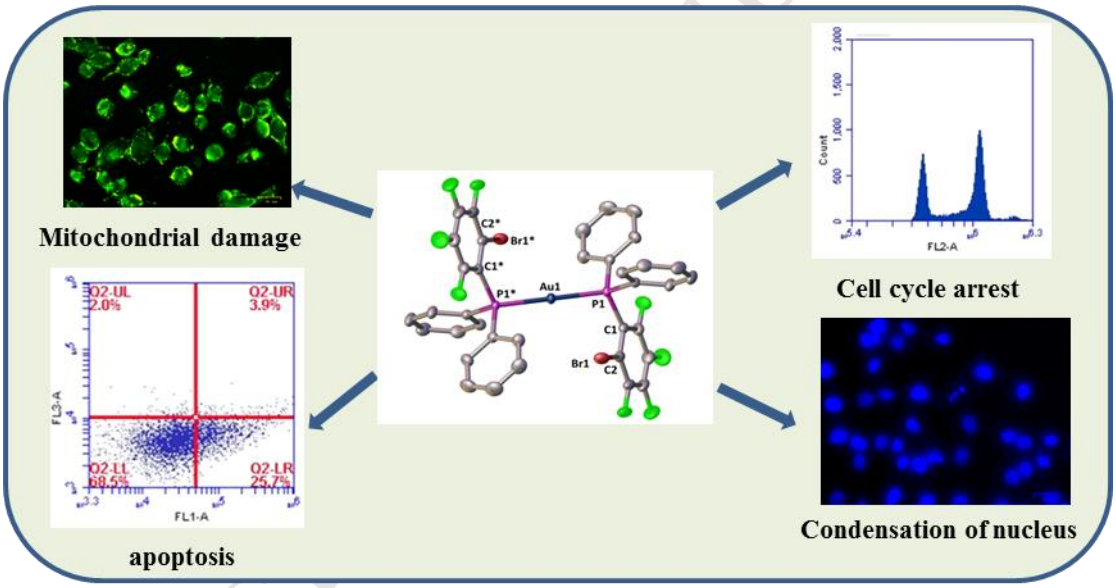

Synthesis of gold(I) phosphine complexes containing the 2-$BrC_6F_4PPh_2$ ligand: Evaluation of anticancer activity in 2D and 3D spheroidal models of HeLa cancer cells

T. Srinivasa Reddy, Steven. H. Privér, Nedaossadat. Mirzadeh,* Suresh. K. Bhargava*

Centre for Advanced Materials & Industrial Chemistry (CAMIC), School of Science, RMIT University, GPO BOX 2476, Melbourne 3001, Australia

Abstract

Newly synthesised mononuclear gold complexes containing the 2-$BrC_6F_4PPh_2$ ligand have been fully characterised and their anticancer activity towards five human tumor [prostate (PC3), glioblastoma (U87MG), cervical (HeLa), fibrosarcoma (HT1080), ovarian (SKOV-3)] and normal human embryonic kidney (Hek-293T) cell lines investigated. Some of the synthesised gold complexes displayed higher cytotoxicity than cisplatin towards PC-3, HeLa and U87MG cells and inhibited the thioredoxin reductase (TrxR) enzyme, which is considered a potential target for new compounds in cancer treatment. The more physiologically relevant tumor spheroid assay demonstrated the superior potency of these gold phosphine complexes in inhibiting the growth of cervical carcinoma cell line HeLa (3D) spheroidal models. The mechanism of cell death was shown to be apoptotic cell death through cell cycle arrest, mitochondrial membrane depolarisation and increased ROS production

Keywords: Gold(I) phosphine complexes; anticancer activity; spheroids; thioredoxin reductase; apoptosis.

*Corresponding authors: e-mail addresses: suresh.bhargava@rmit.edu.au (Suresh. K. Bhargava), nedaossadat.mirzadeh@rmit.edu.au (Nedaossadat. Mirzadeh)

1.0 Introduction

Cancer is a major cause of death worldwide and new drugs are desperately needed in the fight for the treatment of the disease, as almost all drugs used today suffer from severe side effects due to rapid emergence of drug resistance and lack of selectivity towards tumors [1]. Recently, there has been a growing interest in the development of metal-based complexes for the treatment of cancer, mainly because metals exhibit unique characteristics, such as redox activity, variable coordination modes and reactivity toward organic substrates, and have shown promising *in vitro* cytotoxic effects towards various cancer cells [2]. Cisplatin is one of the most widely used metal-based complexes in the treatment of a variety of tumors, including cervical, ovarian, non-small cell lung carcinoma, and testicular cancers. However, the clinical use of cisplatin is hampered by its toxic side-effects, drug resistance and poor solubility. These limitations have led to an intense search for new metal-based agents that show greater selectivity, lower toxicity and improved anticancer activity [3, 4].

Over the last decade, gold complexes have gained attention as an alternative to platinum drugs because of their potential applications in cancer treatment [5]. While the development of anticancer gold(I) complexes has enjoyed an exponential growth, the high redox potential and relatively poor stability of gold(III) complexes have hampered their medicinal applications [6]. Studies on anticancer gold(I) phosphine complexes have continued to accelerate since the discovery that auranofin, which was previously used for the treatment of rheumatoid arthritis [7, 8], has been shown to induce cell death in several cancer cell lines with varying degrees of cytotoxicity [9]. Despite the excellent *in vitro* cytotoxicity, the *in vivo* efficacy of auranofin was limited due to decreased stability in the presence of natural thiols [10]. Intensified research on the development of gold antitumor drugs has led to a number of several other gold(I) phosphine complexes displaying a broad spectrum of anticancer activity, such as

triphenylphosphine gold chloride, [AuCl(PPh_3)], which has been shown to exhibit toxicity towards various cancer cells and induce autophagy [11, 12].

Following our previous studies on gold(I) complexes with anticancer activities [13,14], we were inspired to extend our interest in developing new anticancer complexes based on [AuCl(PPh_3)] containing the 2-$BrC_6F_4PPh_2$ ligand, a well-established ligand used in the development of organogold chemistry [15,16]. In this study, we have investigated the anticancer properties of the newly synthesised gold phosphine complexes (Fig. 1) towards a comprehensive panel of human cancer cell lines and compared the results to those of cisplatin. These complexes were evaluated for their capacity to inhibit the thioredoxin reductase (TrxR) enzyme. Finally, the apoptosis inducing ability of the complexes was also investigated.

<Fig. 1>

2.0 Results and Discussion

2.1 Synthesis of gold complexes:

Reaction of [AuCl(tht)] (tht = tetrahydrothiophene) with an equimolar amount of 2-$BrC_6F_4PPh_2$ afforded the neutral gold(I) chloride complex [AuCl(2-$BrC_6F_4PPh_2$)] (**1**), from which the corresponding bromide (**2**) and iodide (**3**) complexes were prepared by metathetical reaction with LiBr and NaI, respectively (Scheme 1). Abstraction of chloride in **1** by $TlPF_6$ in the presence of one equivalent of 2-$BrC_6F_4PPh_2$ gave the cationic complex [Au(2-$BrC_6F_4PPh_2)_2$]PF_6 (**4**) (Scheme 2). The analogous, previously reported, complex [$Au(PPh_3)_2$]PF_6 (**6**) was prepared similarly from [AuCl(PPh_3)] (**5**) and PPh_3 (Scheme 3) [17].

<Scheme. 1>

<Scheme. 2>

<Scheme. 3>

The new complexes **1-4** were characterised by multinuclear NMR spectroscopy (^{1}H, ^{19}F and ^{31}P, Figs. S1-S14) and their structures confirmed by single crystal X-ray diffraction. In all cases, the ^{1}H NMR spectra are unremarkable and each show the expected aromatic multiplet resonances between δ 7.5-7.8. Similarly, the ^{19}F NMR spectra each show the expected aromatic fluorine resonances in the δ -120 to -150 region, split into multiplets due to complex F-F and F-P coupling. In the case of complex **4**, an additional resonance at δ -73 was also present assignable to the PF_6 counter ion (J_{PF} = 714 Hz). The ^{31}P NMR spectra for complexes **1-4** each show a single broad resonance with unresolved P-F coupling in the δ 30-39 region; the spectrum for **4** also showed the characteristic septet (J_{PF} = 712 Hz) at δ -144 due to PF_6.

The molecular structures of complexes **1-4** were confirmed by X-ray diffraction. The structures of **1** and **4** are shown in Figs. 2 and 3, respectively, and those of **2** and **3** in Figs. S15 and S16, respectively. Selected bond distances (Å) and angles (°) are collected in Table 1 and crystal structure refinement details for complexes **1-4** are reported in Tables S1-S2. The structures of **1-4** each consist of a gold(I) atom coordinated by a phosphorus atom of the tertiary phosphine and a halide, or, in the case of **4**, a second phosphorus atom. As expected, the geometry about the gold atom is linear or close to linear (177-180°), with Au–P bond lengths in the range 2.23-2.30 Å. The Au–X bond lengths are typical for gold(I) halide complexes and increase in the order X = Cl (2.28 Å) < Br (2.39 Å) < I (2.54 Å). In all cases, the metrical parameters in **1-4** are comparable to those observed for their triphenylphosphine analogues [$AuX(PPh_3)$] [18, 19] and [$Au(PPh_3)_2$]PF_6 [17].

<Fig. 2>

<Fig. 3>

<Table. 1>

2.2 Stability of gold phosphine complexes:

The ^{31}P NMR spectra of the metal complexes **1-6** in DMSO-d_6 were measured over a period of 72 h to investigate their stability in this solvent. No changes in the spectra over time were observed, indicating the complexes did not undergo reduction to metallic gold or participate in ligand exchange reactions with DMSO (Figs. S17-S38, Supporting Information). The stability of the complexes under physiological-like conditions was estimated by monitoring the electronic spectra of all the synthesised complexes in a buffer solution (50 mM sodium phosphate, 4 mM NaCl, pH 7.4) over 72 h. As shown in Fig. 4, no change in the electronic spectra was observed over time, indicating the complexes are stable under physiological-like conditions.

<Fig. 4>

2.3 Cytotoxicity:

Given the stability of the gold(I) complexes under physiological-like conditions, the *in vitro* anticancer properties were evaluated against five human tumor cell lines [prostate (PC3), glioblastoma (U87MG), cervical (HeLa), fibrosarcoma (HT1080), ovarian (SKOV-3)] and normal human embryonic kidney cells (Hek-293T) and the results compared to those of cisplatin. Cells were incubated with the gold phosphine complexes for 72 h and cell viabilities were measured using the MTT assay [20]. The results of this assay are expressed as IC_{50} values and are shown in Table 2. Most of the synthesised gold phosphine complexes investigated exhibited remarkable cytotoxic properties with some of the complexes displaying better anticancer activity than cisplatin. Among the series, the newly synthesised cationic gold complex **4** and $[Au(PPh_3)_2]PF_6$ (**6**) displayed potent cytotoxicity towards all the tested cancer cell lines with IC_{50} values ranging from 1.23 to 6.12 µM. Notably, lower IC_{50} values were observed for these complexes towards HeLa cancer cells in comparison to

cisplatin, indicating their higher potency. Among the neutral derivatives, the iodo-complex **3** displayed significant cytotoxicity with IC_{50} values of 1.96 and 2.62 µM towards PC3 (prostate) and U87MG (glioblastoma) cancer cell lines, respectively. The chloro- (**1**) and bromo- (**2**) complexes showed moderated growth inhibition towards all the tested cell lines.

<Table. 2>

The metal complexes were also screened for their cytotoxicity against non-tumorigenic Hek-293T cells to determine their selectivity toward cancer cells. As shown in Table 1, complexes **5** and **6** are, respectively, 5 and 2 times more selective towards the HeLa cancer cells compared to healthy cells. Moreover, the iodo-complex **3** was 6 and 4 times more selective towards PC3 and U87MG cancer cells, respectively, compared to Hek-293T cells. The promising cytotoxic activity of the metal complexes towards HeLa cancer cells encouraged us to study their effects at the cellular level.

2.4 Cellular uptake of gold complexes

As it has been shown that the cellular uptake ability of gold complexes can have an influence on their cytotoxicity [11], we used inductively coupled plasma–mass spectrometry (ICP-MS) to analyse the cellular uptake of complexes **1**-**4** and **6**. In this assay, the amount of gold taken up by the HeLa cells was analysed after 18 h exposure to IC_{50} concentrations of the gold complexes. As shown in Fig. 5, after 18 h incubation, the bromo complex **2** entered the cells with similar efficiency to the iodo complex **3**. In contrast, the cellular uptake of the chloro complex **1** was 3 times lower than that of the bromo and iodo complexes. As expected, the highly cytotoxic cationic complexes **4** and **6** were efficiently internalised in the cells with 5-15 fold higher amounts than the neutral complexes. These results are clearly in agreement with the anticancer activity of the metal complexes.

<Fig. 5>

2.5 Spheroid inhibition assay

3D Multicellular spheroids closely reflect the *in vivo* tumor environment with respect to nutrient and oxygen gradients, phenotypic heterogeneity, micrometastases and gene expression profiles [21]. Therefore, we examined the effect of the gold phosphine complexes on the 3D multicellular spheroids of HeLa. Spheroids grown in ultra-low attachment plates for 3 days were treated with the gold phosphine complexes for a period of 96 h and were examined for morphological changes. The results showed that all the gold phosphine complexes significantly inhibited the growth of HeLa cell spheroids compared to the untreated control cells. This effect was more prominent for complexes **2**, **4** and **6**, with complex **4** being particularly effective at inhibiting tumor spheroid growth (Fig. 6).

<Fig. 6>

2.6 TrxR/GR inhibition assay

The thioredoxin system, composed of thioredoxin reductase (TrxR), thioredoxin (Trx), and NADPH (nicotinamide adenine dinucleotide phosphate), is associated with maintaining and regulating cellular redox homeostasis [22]. Overexpression of TrxR in many tumor cells contributes to increased drug resistance [23]. Thus, inhibition of TrxR has emerged as a new target for anticancer drugs and gold complexes have been shown to be potent TrxR inhibitors [24-26]. Therefore, in order to investigate the TrxR inhibitory activities of the gold phosphine complexes, the DTNB [5,5'-dithio-bis-(2-nitrobenzoic acid)] assay was carried out [27]. In this assay, DTNB is used as a TrxR substrate that is reduced to 2-nitro-5-thiobenzoic acid (TNB) in the presence of NADPH. The rate of conversion of DTNB to TNB is reflective of TrxR activity and was monitored by UV-Visible spectrometry at 412 nm. The calculated IC_{50} values are shown in Table 3. All of the gold phosphine complexes exhibited significant TrxR

inhibitory activity with EC_{50} values of 0.08-0.28 µM, except for the cationic gold complexes **4** and **6**, which showed moderate inhibition with EC_{50} values of 2.6-3.5 µM. A possible explanation for the decreased TrxR inhibitory activity of the cationic gold complexes over the neutral complexes may be due to the absence of labile halide ligands, which may participate in ligand exchange reactions with the selenium-containing amino acid selenocysteine within the active site of the TrxR enzyme. Indeed, these cationic complexes showed potent cytotoxicity among the series, indicating a different cell growth inhibition mechanism other than TrxR inhibition.

<Table. 3>

2.7 Cell cycle analysis:

The effect of the metal complexes on the cell cycle distribution of HeLa cells was examined by flow cytometric analysis of the cellular DNA content. HeLa cells were treated with IC_{50} concentrations of the gold complexes for 48 h. The cells were stained with propidium iodide (PI) and the DNA content was analysed using flow cytometry. The results are expressed as the percentage cell population in each phase of the cell cycle and are shown in Fig. 7. The results show that after 48 h of treatment with the gold complexes, accumulation of cells in the G0/G1 phase with a concomitant loss of cells in the S and G2/M phases had taken place. The effect is more prominent after treatment with complexes **2** and **5**, with approximately 73% of cells in the G0/G1 phase compared to only 47% for the control cells, indicating G0/G1 phase cell cycle arrest in HeLa cells. In stark contrast, treatment with the cationic gold complexes **4** and **6** resulted in accumulation of cells in the G2/M phases, further supporting a different mode of action for these complexes.

<Fig. 7>

2.8 Hoechst staining:

Because arresting cell cycle progression can result in the initiation of apoptosis [28], we next investigated the apoptosis inducing ability of complexes **1**-**6** in HeLa cells using Hoechst 33242 nuclear staining. To examine this, HeLa cells were treated with IC_{50} concentrations of the complexes, stained with Hoechst 33242, and examined for nuclear morphological changes by fluorescence microscopy. The results showed that treatment with complexes **1**-**6** resulted in condensation of nuclei (brightly stained), as indicated by the arrows in Fig. 8, while the control cells exhibited uniformly dispersed chromatin. Moreover, fragmented nuclei can also be seen in the cells treated with complexes **1**, **4**, **6** and cisplatin. These results indicate that the metal complexes induce apoptosis in HeLa cells.

<Fig. 8>

2.9 Assessment of mitochondrial membrane potential:

To investigate whether apoptosis induced by metal complexes was mediated through mitochondrial damage, we measured the mitochondrial outer membrane potential in HeLa cells using JC-1 (5,5′,6,6′-tetrachloro-1,1′,3,3′-tetraethylbenzimidazolocarbocyanine iodide). JC-1 is a mitochondrial-selective fluorescent dye which emits red fluorescence (J-aggregates) in normal mitochondria and green fluorescence (J-monomers) in damaged mitochondria as the membrane potential decreases due to apoptosis [29]. Fluorescence microscopic imaging analysis using JC-1 showed that after 48 h, HeLa cells treated with the metal complexes (**1**-**6**) exhibited higher JC-1 green fluorescence with lower red fluorescence compared to the untreated cells (Fig. 9). The mitochondria in the control cells were intact and emitted red fluorescence after JC-1 staining. These results indicate disruption of mitochondrial membrane integrity and loss of mitochondrial membrane potential in the treated cells.

<Fig. 9>

2.10 Reactive Oxygen Species (ROS)

Several studies have demonstrated that mitochondrial damage leads to increased production of reactive oxygen species (ROS) [30]. Therefore, it was of interest to investigate whether the mitochondrial damage induced by the gold complexes would lead to increased ROS generation. HeLa cells were treated with IC_{50} concentrations of the gold complexes for 48 h, stained with a ROS-sensitive fluorogenic dye (dichlorodihydrofluorescein diacetate, DCF-DA) and analysed by flow cytometry. The results, shown in Fig. 10, indicate that the cells treated with the metal complexes generated 1.8 to 3.5 times more intracellular ROS compared to the control cells, with the cationic complexes **4** and **6** being particularly effective.

<Fig. 10>

2.11 Annexin V-FITC/propidium iodide double staining assay

Phosphatidylserine (PS) externalisation on the outer leaflet of the plasma membrane occurs during the early stages of apoptosis and can be detected using fluorescein-labelled Annexin V (Annexin V-FITC), a Ca^{2+}-dependent phospholipid binding protein with a high affinity for PS [31]. To quantify the apoptosis induced by the metal complexes in HeLa cells, and to differentiate the cell death induced by the metal complexes due to necrosis or apoptosis, the Annexin V-FITC/PI dual staining assay was carried out. In this assay, HeLa cells treated with the metal complexes were stained with Annexin V-FITC and PI and analysed for their fluorescence by flow cytometry. As shown in Fig. 11, the percentage of early apoptotic cells and late apoptotic cells increased after treatment with the metal complexes (19-33%) compared to the control cells (12.3%). Treatment with the cationic complexes **4** and **6** resulted in higher amounts of cells stained with Annexin (early apoptotic cells) and PI-positive (late apoptotic cells). The total percentage of apoptotic cells (sum of early apoptotic cells and late apoptotic cells) in HeLa cells increased from 12.1% to 29.6 and 26.6% after

treatment with complexes **4** and **6**, respectively. From these results, it can be concluded that the metal complexes induce extensive apoptosis in HeLa cells.

<Fig. 11>

3.0 Conclusions

In this study we have synthesised a series of neutral and cationic gold phosphine complexes containing the 2-$BrC_6F_4PPh_2$ ligand and investigated their ability to inhibit the growth of five human tumor cell lines and one normal cell line. The metal complexes displayed significant stability under physiological-like conditions and anti-proliferative properties. The neutral complexes (**1-3**) displayed moderate cytotoxicity towards all the tested cancer cell lines with IC_{50} values in the range 6.51-22.5 µM. Remarkably, the cationic complexes **4** and **6** showed potent and higher cytotoxicity than cisplatin, with IC_{50} values of 1.9 and 1.2 µM, respectively, towards HeLa cancer cells. These cationic complexes tend to accumulate in higher amounts in the cancer cells than the neutral complexes, leading to higher cytotoxicity. The metal complexes displayed significant inhibitory activities on solid tumor cell proliferation (HeLa spheroids). Treatment of HeLa cells with the neutral complexes resulted in G0/G1 cycle arrest whereas the cationic complexes caused G2/M cell cycle arrest. Hoechst 33342 staining demonstrated that the metal complexes effectively induced apoptosis of HeLa cells. In addition, these complexes enhanced the level of intracellular ROS and induced a decrease of mitochondrial membrane potential. Taken together all these results suggest that the metal complexes induce apoptosis in HeLa cells through mitochondrial membrane depolarisation and increased ROS accumulation and ROS mediated DNA damage. Moreover, the neutral metal complexes strongly inhibited thioredoxin reductase (TrxR) with lower activity towards glutathione reductase (GR) while the cationic complexes displayed moderate

TrxR inhibition, demonstrating their great potential in anticancer drug discovery and development.

4.0 Experimental

4.1 General comments

The compounds 2-$BrC_6F_4PPh_2$ [32, 33], [AuCl(tht)] [34], and [$AuCl(PPh_3)$] [35] were prepared following literature methods, and [$Au(PPh_3)_2$]PF_6 by a slightly modified literature method [17], the details of which are given below. ^{1}H (300 MHz), ^{19}F (282 MHz) and ^{31}P (121 MHz) NMR spectra were measured as $CDCl_3$ solutions on a Bruker Avance 300 spectrometer at room temperature. For the stability studies, DMSO-d_6 was used. Chemical shifts are referenced to residual solvent signals (^{1}H), $CFCl_3$ (^{19}F) or external 85% H_3PO_4 (^{31}P) and coupling constant (J) are given in Hz.

4.1.1 X-ray Crystallography

Crystals of complexes **1**-**4** suitable for single-crystal X-ray diffraction were obtained from dichloromethane/hexane. Using a drop of inert oil (Nujol), crystals were mounted on a nylon loop and transferred into a stream of cold nitrogen. The reflections were collected on a D8 Bruker diffractometer equipped with an APEX-II area detector using graphite-monochromated Mo Kα radiation (λ = 0.71073 Å) from a 1 μS microsource. The computer programs SMART [36] and SAINT [37] were used for data collection in φ- and ω- scan modes and data processing, respectively, and absorption corrections using SADABS [38]. The structures were solved using direct methods and refined with full-matrix least-squares methods on F^2 using the SHELX-TL package [39, 40]. The computer program OLEX2 was used to generate the X-ray crystal structures [41]. The CCDC numbers for complexes **1-4** are 1582742-1582745.

4.1.2 Preparation of [AuCl(2-$BrC_6F_4PPh_2$)] (1)

To a solution of [AuCl(tht)] (305 mg, 0.95 mmol) in CH_2Cl_2 (20 mL) cooled to 0 °C was added 2-$BrC_6F_4PPh_2$ (393 mg, 0.95 mmol). After stirring for 15 min the solution was warmed to room temperature and filtered through Celite. MeOH was added to the filtrate and the volume of the solution was reduced, precipitating a white solid, which was filtered off, washed with MeOH and dried *in vacuo* (535 mg, 87%). ^{1}H NMR: δ 7.48-7.57 (m, 4H), 7.58-7.73 (m, 6H). ^{31}P NMR: δ 30.2 (m). ^{19}F NMR: δ -122.8 (m), -124.2 (m), -145.0 (m), -151.7 (m).

4.1.3 Preparation of [AuBr(2-$BrC_6F_4PPh_2$)] (2)

To a solution of [AuCl(2-$BrC_6F_4PPh_2$)] (200 mg, 0.31 mmol) in CH_2Cl_2 (30 mL) was added a solution of LiBr (45 mg, 0.52 mmol) in MeOH (15 mL) and the solution was stirred for 15 min. The solvent was removed *in vacuo* and the residue dissolved in CH_2Cl_2. After filtration through Celite, MeOH was added to the filtrate and the volume of the solution was reduced *in vacuo*. The white precipitate was filtered off, washed with MeOH and dried *in vacuo* (190 mg, 89%). ^{1}H NMR: δ 7.48-7.57 (m, 4H), 7.58-7.73 (m, 6H). ^{31}P NMR: δ 32.3 (m). ^{19}F NMR: δ -122.9 (m), -124.2 (m), -145.0 (m), -151.7 (m).

4.1.4 Preparation of [AuI(2-$BrC_6F_4PPh_2$)] (3)

This was prepared analogously to the bromo complex above from [AuCl(2-$BrC_6F_4PPh_2$)] (200 mg, 0.31 mmol) and NaI (70 mg, 0.47 mmol) to give the product as a white solid (201 mg, 88%). ^{1}H NMR: δ 7.48-7.58 (m, 4H), 7.59-7.75 (m, 6H). ^{31}P NMR: δ 36.1 (m). ^{19}F NMR: δ -123.0 (m), -124.2 (m), -145.2 (m), -151.8 (m).

4.1.5 Preparation of [Au(2-$BrC_6F_4PPh_2$)$_2$]PF_6 (4)

To a solution of [AuCl(2-$BrC_6F_4PPh_2$)] (100 mg, 0.15 mmol) and 2-$BrC_6F_4PPh_2$ (64 mg, 0.15 mmol) in CH_2Cl_2 (8 mL) was added $TlPF_6$ (55 mg, 0.16 mmol) and the mixture was stirred for 1.5 h in the dark. The suspension was filtered through Celite, hexane was added to the filtrate and the volume of the solution was reduced *in vacuo*. The white solid that precipitated

was filtered off, washed with hexane and dried *in vacuo* (156 mg, 86%). ^{1}H NMR: δ 7.54-7.74 (m, 20H). ^{31}P NMR: δ 38.8 (br m), -144.8 (sept, J_{PF} = 712 Hz). ^{19}F NMR: δ -73.4 (d, J_{PF} = 714 Hz), -122.8 (m, 2F), -143.3 (m), -150.5 (m).

4.1.6 Preparation of $[Au(PPh_3)_2]PF_6$ (6)

To a solution of $[AuCl(PPh_3)]$ (85 mg, 0.17 mmol) and PPh_3 (45 mg, 0.17 mmol) in CH_2Cl_2 (8 mL) was added $TlPF_6$ (63 mg, 0.18 mmol) and the mixture was stirred for 1.5 h in the dark. The suspension was filtered through Celite, hexane was added to the filtrate and the volume reduced *in vacuo*. The white solid that precipitated was filtered off, washed with hexane and dried *in vacuo* (146 mg, 97%). ^{1}H NMR: δ 7.47-7.73 (m, 30H). ^{31}P NMR: δ 45.1 (s), -144.3 (sept, J_{PF} = 713 Hz).

4.2 Stability of the metal complexes in DMSO and physiological-like conditions

The stability of the complexes in phosphate buffer saline (PBS) was monitored using UV-Visible absorption spectroscopy. The UV-Vis absorption spectra of the gold complexes were recorded on a Varian Cary 50 UV-Visible spectrophotometer. Stock solutions of the metal complexes were freshly prepared in DMSO and diluted to 25 µM in PBS buffer. The absorption spectra of 25 µM gold complexes in PBS were monitored over time, from 0 h to 72 h. ^{1}H NMR and ^{31}P NMR experiments of the gold complexes were carried out in DMSO-d_6 and monitored over time to determine their stability in DMSO.

4.3 Cell Culture

Prostate (PC-3), glioblastoma (U87MG), cervical (HeLa), fibrosarcoma (HT1080), ovarian (SKOV-3) and human embryonic kidney (Hek-293T) cells were purchased from ATCC. PC-3 and HeLa cells were grown in RPMI medium, whereas U87MG, HT1080, SKOV-3, and Hek-293T were maintained in DMEM medium supplemented with 10% FBS and 1% PS. All cells were maintained in a sterile incubator with 75% humidity and 5% CO_2 at 37 ^{o}C. Cells

were harvested with 0.25% trypsin-ethylenediaminetetraacetic acid (EDTA, Life Technologies) for subculture and plating after reaching 80% confluence. For all the assays, unless otherwise mentioned, stock solutions of the metal complexes were freshly prepared in DMSO (10 mM) and 1% DMSO in complete medium was used as a control. Cisplatin (positive control) was purchased from Sigma-Aldrich.

4.3.1 MTT assay

The MTT [3-(4,5-dimethylthiazol-2-yl)-2,5-diphenyltetrazolium bromide] assay is based on the conversion of a yellow coloured MTT solution to purple formazan crystals by the active mitochondrial dehydrogenases of viable cells. Thus, the intensity of the produced purple colour is proportional to the number of viable cells. The cells were seeded in 96 well plates depending on cellular doubling time and were treated with solutions of the metal complexes (100 µM, 10 µm, 1 µM, 0.1 µM, 0.01 µM) after overnight incubation. The cells were further incubated for 48 h and the medium containing the test compounds was removed before addition of 100 µL MTT solution (5 mg/mL) in serum-free medium. After 4 h incubation in the dark at 37 °C, the excess MTT solution was removed from the wells and 100 µL of DMSO was added to each well to solubilise the formed formazan crystals. The absorbance of formazan solution from each well was recorded using a Spectramax micro titre plate reader at 570 and 630 nm. Growth inhibition of the compounds was calculated as IC_{50} values (concentration of compound that causes 50% inhibition of cell growth) using Probit software. Each experiment was repeated three time and the standard deviation values are reported in Table 2.

4.3.2 Spheroid assay. HeLa cells at low densities of 25000 per well were seeded in a Corning® Costar® Ultra-Low attachment 24 well plate in complete growth medium and allowed to incubate for 3 days to form spheroids. The cells were treated with IC_{50}

concentrations of metal complexes and the growth of the spheroids was monitored after 48 and 96 h using a phase contrast microscope.

4.3.3 TrxR (thioredoxin reductase) inhibition assay

In this assay, 25 μL of the various concentrations of metal complexes (10 μM, 5 μM, 2.5 μM, 1.25 μM, 0.62 μM, dissolved in DMSO: phosphate buffer) was incubated with 25 μL of TrxR or GR enzyme (2.0 U/mL in milliQ water) in a 96 well plate. After incubation for 30 min at 37 °C, 200 μL of reaction mixture (1000 μL of mixture contains 500 μL phosphate buffer pH 7.0, 80 μL of EDTA solution 100 mM pH 7.5, 20 μL of BSA [bovine serum albumin] solution of 0.2%, 400 μL of distilled water) was added to each well and then 25 μL of 20 mM NADPH (nicotinamide adenine dinucleotide phosphate) solution was added. Finally, 25 μL of 20 mM ethanolic DTNB [5,5′-dithiobis-(2-nitrobenzoic acid)] was added and the increased absorbance due to the formation of TNB (2-nitro-5-thiobenzoic acid) was recorded immediately at 412 nm for 10 min with 30 s intervals using a SpectraMax plate reader. 1 unit of enzyme activity was defined as 1 μmol of NADPH oxidised per min using the formula ΔA405nm × 1 / (13.6 × 2), where 1 mol of NADPH yields 2 mol of TNB. Data are the means of triplicate of three independent experiments [27].

4.3.4 Cell Cycle analysis

HeLa cells were plated in a 6 well plate at a density of 1×10^6/well and allowed to adhere overnight in an incubator. Cells were treated with IC_{50} concentrations of complexes **1**-**6** and cisplatin for a period of 48 h and were collected by trypsinisation, washed with PBS and fixed with 70% ethanol. After fixation, cells were stained with propidium iodide staining solution and kept in ice till analysis. 10000 cells from each sample were analysed for propidium iodide fluorescence in FL-2 channel mode using a BD Accuri C6 flow cytometer [42].

4.3.5 Hoechst staining

The nuclear morphological changes in the HeLa cells were assessed using Hoechst 33242. In this assay, HeLa cells were grown on coverslips in 6 well plates and treated with IC_{50} concentrations of complexes **1-6** and cisplatin for 48 h. The culture medium was removed, the cells washed with PBS, fixed with 4% paraformaldehyde at room temperature for 20 min and stained with 2 µg/mL Hoechst 33242. The excess dye was removed after 20 min incubation and the cells were washed three times with PBS. The cells were observed for their nuclear morphological changes under a confocal microscope using 20x lens (NIKON) [43].

4.3.6 Assessment of mitochondrial membrane potential

HeLa cells were seeded in 24 well plates at a density of 5×10^5 cells/mL and treated with complexes **1-6** and cisplatin. After 48 h incubation, the medium was removed and the cells were washed with PBS and 500 µL of fresh medium containing 5 µg/mL JC-1 was added. Cells were washed three times with PBS after incubating for 20 min and photographed at a magnification of 20× using a fluorescence microscope (BIORAD) [44].

4.3.7 Intracellular reactive oxygen species

The intracellular levels of reactive oxygen species were measured using DCFDA staining. Briefly, HeLa cells were treated with IC_{50} concentrations of complexes **1-6** and cisplatin for 48 h. After treatment, the cells were collected by trypsinisation, washed with PBS, and stained with Carboxy-DCFDA (10 µM). 5000 cells from each sample were analysed for the green fluorescence of DCF using a BD Accuri C6 cytometer [45].

4.3.8 Annexin-V FITC/propidium iodide double staining

HeLa cells (1×10^6/well) were grown in 6 well plates and incubated with IC_{50} concentrations of complexes **1-6**. After 48 h, the cells were collected by trypsinisation and washed with PBS.

The cells were resuspended in Annexin binding buffer and 5 μL of Annexin and 1 μL of PI was added to each sample and incubated for 15 min at room temperature. 15000 cells from each sample were analysed immediately using a BD Accuri C6 flow cytometer [46].

Acknowledgements

The authors acknowledge the Micro Nano Research Facility (MNRF), RMIT University for providing the facilities to carry out these experiments.

5.0 References

[1] H. Newell, E. Sausville, Cytotoxic drugs: past, present and future, Cancer Chemother. Pharmacol. 77 (2016) 1.

[2] Z.F. Chen, C. Orvig, H. Liang, Multi-target metal-based anticancer agents, Curr. Top. Med. Chem. 17 (2017) 3131-3145.

[3] A.M. Florea, D. Büsselberg, Cisplatin as an anti-tumor drug: Cellular mechanisms of activity, drug resistance and induced side effects, Cancers 3 (2011) 1351–1371.

[4] D. Gibson, The mechanism of action of platinum anticancer agents-what do we really know about it?, Dalton Trans. 48 (2009) 10681–10689.

[5] C. Nardon, G. Boscutti, D. Fregona, Beyond, platinums: gold complexes as anticancer agents, Anticancer Res. 34 (2014) 487–492.

[6] T. Zou, C.T. Lum, C.N, Lok, J.J. Zhang, C.M. Che, Chemical biology of anticancer gold(III) and gold(I) complexes, Chem. Soc. Rev. 44 (2015) 8765–8942.

[7] J. Forestier, Rheumatoid arthritis and its treatment by gold salts, J. Lab. Clin. Med. 20 (1935) 827–840.

[8] C.K Mirabelli, R.K Johnson, D.T Hill, L.F Faucette, G.R Girard, G.Y Kuo, C.M Sung, S.T. Crooke, Correlation of the *in vitro* cytotoxic and *in vivo* antitumor activities of gold(I) coordination complexes, J. Med. Chem. 29 (1986) 218–223.

[9] T. Marzo, D. Cirri, C. Gabbiani, T. Gamberi, F. Magherini, A. Pratesi, A. Guerri, T. Biver, F. Binacchi, M. Stefanini, A. Arcangeli, L. Messori, Auranofin, Et_3PAuCl, and Et_3PAuI are Highly cytotoxic on colorectal cancer cells: A chemical and biological study, ACS Med. Chem. Lett. 8 (2017), 997–1001.

[10] F. Di Sarra, B. Fresch, R. Bini, G. Saielli, A. Bagno, Reactivity of auranofin with selenols and thiols: implications for the anticancer activity of gold(I) compounds, Eur. J. Inorg. Chem. (2013), 2718–2727.

[11] H. Scheffler, Y. You, I. Ott, Comparative studies on the cytotoxicity, cellular and nuclear uptake of a series of chloro gold(I) phosphine complexes, Polyhedron 29 (2010) 66–69.

[12] S. Tian, F.M. Siu, S.C.F. Kui, C.N. Lok, C.M. Che, Anticancer gold(I)–phosphine complexes as potent autophagy-inducing agents, Chem. Commun. 47 (2011) 9318–9320.

[13] N. Mirzadeh, S.H. Privér, A. Abraham, R. Shukla, V. Bansal, S.K. Bhargava, Linking flavonoids to gold–A new family of gold compounds for potential therapeutic applications, Eur. J. Inorg. Chem. 2015 (2015) 4275–4279.

[14] T.S. Reddy, S.H. Privér, N. Mirzadeh, S.K. Bhargava, Anti-cancer gold(I) phosphine complexes: Cyclic trimers and tetramers containing the P-Au-P moiety, J. Inorg. Biochem. 175 (2017) 1–8.

[15] M.A. Bennett, S.K. Bhargava, N. Mirzadeh, S.H. Privér, J. Wagler, A.C. Willis, Synthesis and interconversions of digold(I), tetragold(I), digold(II), gold(I)–gold(III) and digold(III) complexes of fluorine-substituted aryl carbanions, Dalton Trans. 36 (2009) 7537–7551.

[16] N. Mirzadeh, M.A. Bennett, S.K. Bhargava, Cycloaurated complexes of aryl carbanions: digold(I), digold(II) and beyond, Coord. Chem. Rev. 257 (2013) 2250–2273.

[17] R.J. Staples, C.King, M.N.I. Khan, R.E.P. Winpenny, J.P. Fackler Jr., Structures of bis(triphenylphosphine) gold(I) hexafluorophosphate, $[Au(PPh_3)_2]PF_6$ (1), and bis (triphenylphosphine) gold(I) nitrate, $[Au\ (PPh_3)_2]NO_3$ (2), Acta Cryst. 49 (1993) 472–475.

[18] N.C. Baenziger, W.E. Bennett, D.M. Soborofe, Chloro (triphenylphosphine) gold(I), Acta Crystallogr. B32 (1976) 962-963

[19] P.F. Barron, L.M. Engelhardt, P.C. Healy, J. Oddy, A.H. White, Lewis-Base Adducts of Group I Metal(I) Compounds. XXVI. Solid-State Cross-Polarization Magic-Angle-Spinning ^{31}P N.M.R. and Structural Studies on 1:1 Adducts of Triphenylphosphine With Gold(I) Salts, Aust. J. Chem. 40 (1987) 1545-1555.

[20] D. Gerlier, N. Thomasset, Use of MTT colorimetric assay to measure cell activation, J. Immunol. Methods. 94 (1986) 57–63.

[21] J. Wang, X. Zhang, X. Li, Y. Zhang, T. Hou, L. Wei, L. Qu, L. Shi, Y. Liu, L. Zou, X. Liang, Anti-gastric cancer activity in three-dimensional tumor spheroids of bufadienolides, Sci. Rep. 6 (2016) 24772.

[22] D. Mustacich, G. Powis, Thioredoxin reductase, Biochem. J. 346 (2000) 1–8.

[23] J. Wang, M. Kobayashi, K. Sakurada, M. Imamura, T. Moriuchi, M. Hosokawa, Possible roles of an adult T-cell leukemia (ATL)-derived factor/thioredoxin in the drug resistance of ATL to Adriamycin, Blood 89 (1997) 2480–2487.

[24] N. Shaik, A. Martinez, I. Augustin, H. Giovinazzo, A. Varela-Ramirez, M. Sanau, R.J. Aguilera, M. Contel, Synthesis of Apoptosis-Inducing Iminophosphorane Organogold(III) Complexes and Study of Their Interactions with Biomolecular Targets, Inorg. Chem., 48 (2009) 1577–1587.

[25] G.L. Parrilha, K.S. Ferraz, J.A. Lessa, K.N. de Oliveira, B.L Rodrigues, J.P Ramos, E.M. Souza-Fagundes, I. Ott, H. Beraldo, Metal complexes with 2-acetylpyridine-N(4)-orthochlorophenylthiosemicarbazone: Cytotoxicity and effect on the enzymatic activity of thioredoxin reductase and glutathione reductase, Eur. J. Med. Chem. 84 (2014) 537–544.

[26] Y.F. Mui, J. Fernandez-Gallardo, B.T. Elie, A. Gubran, I. Maluenda, M. Sanau, O. Navarro, M. Contel, Titanocene−Gold Complexes Containing N‑Heterocyclic Carbene Ligands Inhibit Growth of Prostate, Renal, and Colon Cancers *in Vitro*, Organometallics 35 (2016) 1218–1227.

[27] R. Rubbiani, I. Kitanovic, H. Alborzinia, S. Can, A. Kitanovic, L.A. Onambele, M. Stefanopoulou, Y. Geldmacher, W.S. Sheldrick, G. Wolber, A. Prokop, S. Wolfl, I. Ott, Benzimidazol-2-ylidene gold(I) complexes are thioredoxin reductase inhibitors with multiple antitumor properties, J. Med. Chem. 53 (2010) 8608–8618.

[28] C. Praveen Kumar, T.S. Reddy, P.S. Mainkar, V. Bansal, R. Shukla, S. Chandrasekhar, H.M. Hügel, Synthesis and biological evaluation of 5,10-dihydro-11H-dibenzo[b,e][1,4]diazepin-11-one structural derivatives as anticancer and apoptosis inducing agents, Eur. J. Med. Chem. 108 (2016) 674–686.

[29] S. Salvioli, A. Ardizzoni, C. Franceschi, A. Cossarizza, JC-1, but not $DiOC_6(3)$ or rhodamine 123, is a reliable fluorescent probe to assess $\Delta\Psi$ changes in intact cells: implications for studies on mitochondrial functionality during apoptosis, FEBS Lett. 411 (1997) 77–82.

[30] A.J Kowaltowski, A.E Vercesi, Mitochondrial damage induced by conditions of oxidative stress, Free Radic. Biol. Med. 26 (1999) 463–471.

[31] M. Engeland, L.J.W. van Nieland, F.C.S. Ramaekers, B. Schutte, C.P.M. Reutelingsperger. Annexin V-affinity assay: a review on an apoptosis detection system based on phosphatidylserine exposure, Cytometry 31 (1998) 1–9.

[32] P.G. Eller, D.W. Meek, Syntheses of new tetrafluoroaryl derivatives of phosphorus and sulphur, J. Organomet. Chem. 22 (1970) 631–636.

[33] M.A. Bennett, S.K. Bhargava, M.A. Keniry, S.H. Privér, P.M. Simmonds, J. Wagler, A.C. Willis, A triad of bis(orthometalated) d^8-complexes containing four-membered rings, Organometallics 27 (2008) 5361–5370.

[34] R. Uson, A. Laguna, M. Laguna, (Tetrahydrothiophene)gold(I) or gold(III) complexes, Inorg. Synth. 26 (1989) 85–91.

[35] A. Adé, E. Cerrada, M. Contel, M. Laguna, P. Merino, T. Tejero, Organometallic gold(III) and gold(I) complexes as catalysts for the 1,3-dipolar cycloaddition to nitrones: synthesis of novel gold–nitrone derivatives, J. Organomet. Chem. 689 (2004) 1788–1795.

[36] SMART software ver. 5.625 for the CCD Detector System, Bruker AXS Inc.: Madison, WI, 2001.

[37] SAINTPLUS software ver. 6.22 for the CCD Detector System, Bruker AXS Inc.: Madison, WI, 2001.

[38] R.H. Blessing, An empirical correction for absorption anisotropy, Acta Crystallogr. Sect A 51 (1995) 33–38.

[39] G.M. Sheldrick, SHELXTL, ver. 2013/4, Universität Göttingen, Germany, 2013.

[40] G.M. Sheldrick, A short history of SHELX, Acta Crystallogr. Sect A 64 (2008) 112–122.

[41] O.V. Dolomanov, L.J. Bourhis, R.J. Gildea, J.A.K. Howard, H. Puschmann, OLEX2: a complete structure solution, refinement and analysis program, J. Appl. Crystallogr. 42 (2009) 339–341.

[42]) T.S. Reddy, V.G. Reddy, H. Kulhari, R. Shukla, A. Kamal, V. Bansal, Synthesis of (Z)-1-(1,3-diphenyl-1H-pyrazol-4-yl)-3-(phenylamino)prop-2-en-1-one derivatives as potential anticancer and apoptosis inducing agents, Eur. J. Med. Chem. 117 (2016) 157–166.

[43] V.G. Reddy, T.S. Reddy, V.L. Nayak, B. Prasad, A.P. Reddy, A. Ravikumar, S. Taj, A. Kamal, Design, synthesis and biological evaluation of N-((1-benzyl-1H-1,2,3-triazol-4-yl)methyl)-1,3-diphenyl-1H-pyrazole-4-carboxamides as CDK1/Cdc2 inhibitors, Eur. J. Med. Chem. 122 (2016) 164–177.

[44] Y. Ye, T. Zhang, H. Yuan, D. Li, H. Lou, P. Fan, Mitochondria-targeted lupane triterpenoid derivatives and their selective apoptosis-inducing anticancer mechanisms, J. Med. Chem, 60 (2017) 6353–6363.

[45] F. Dai, Q. Li , Y. Wang, C. Ge, C. Feng , S. Xie, H. He, X. Xu, C. Wang, Design, synthesis, and biological evaluation of mitochondria-targeted flavone–naphthalimide–polyamine conjugates with antimetastatic activity, J. Med. Chem. 60 (2017) 2071–2083.

[46] N.P. Kumar, P. Sharma, T.S. Reddy, S. Nekkanti, N. Shankaraiah, G. Lalita, S. Sujanakumari, S.K. Bhargava, V.G.M. Naidu, A. Kamal, Synthesis of 2,3,6,7-tetramethoxyphenanthren-9-amine: An efficient precursor to access new 4-aza-2,3-

dihydropyridophenanthrenes as apoptosis inducing agents, Eur. J. Med. Chem. 127 (2017) 305–317.

Figure/Schemes/Table captions

Fig. 1. Structures of the gold(I) phosphine complexes used in this investigation.

Scheme 1. Synthesis of neutral gold(I) complexes (**1-3).**

Scheme 2. Synthesis of a cationic gold(I) complex (**4**).

Scheme 3. Synthesis of a cationic gold(I) complex (**6**).

Fig. 2. Molecular structure of [AuCl(2-$BrC_6F_4PPh_2$)] (**1**). Ellipsoids show 50% probability levels and hydrogen atoms have been omitted for clarity. Only one molecule in the asymmetric unit is shown.

Fig. 3. Molecular structure of the cation in [Au(2-$BrC_6F_4PPh_2)_2$]PF_6 (**4**). Ellipsoids show 50% probability levels. Hydrogen atoms and PF_6 counter ion have been omitted for clarity. Only one molecule in the asymmetric unit is shown.

Fig. 4. UV-Vis absorption spectra of the gold(I) complexes (25 µM) in sodium phosphate buffer (50 mM, pH 7.4) over 72h.

Table 1. Selected bond distances (Å) and angles (º) in complexes **1-4**.

Table 2. IC_{50} values (µM)* of the gold phosphine complexes against selected human cancer cell lines and normal cell line (Hek-293T).

Table 3. Thioredoxin reductase (TrxR) and glutathione reductase (GR) inhibition activity (EC_{50}, µM)* of the gold phosphine complexes **1–6**.

Fig. 5. The amount of gold taken up by cervical cancer cells (HeLa) after exposure to IC_{50} concentrations of the gold complexes for 24 h.

Fig. 6. Effect of complexes **1-6** and cisplatin on HeLa spheroid formation. HeLa cells were grown in ultra-low attachment plates and treated with IC_{50} concentrations of the metal complexes for the spheroid assay. After 48 h and 96 h, the spheroids were photographed.

Fig. 7. Cell cycle distribution of HeLa cells after treatment with the gold complexes **1-6** and cisplatin for 48 h. The percentage of cells in each phase was analysed using BDC6 accuri software.

Fig. 8. Apoptosis in HeLa cells induced by complexes **1-6** and cisplatin, observed using Hoechst 33242 staining. HeLa cells were incubated with IC_{50} concentrations of the complexes for 48 h. The morphological changes of cell apoptosis such as condensation of chromatin and nuclear fragmentations were observed by fluorescence microscopy after staining with Hoechst 33242.

Fig. 9. Fluorescence microscopic images of mitochondrial membrane integrity disruption in HeLa cells induced by treatment with complexes **1-6**. HeLa cells were treated with IC_{50} concentrations of the metal complexes for 48 h before staining with JC-1 and were imaged by fluorescence microscopy.

Fig. 10. Metal complex induced production of intracellular ROS in HeLa cancer cells. Cells were treated with IC_{50} concentrations of the metal complexes for 48 h, stained with 10 μM DCF-DA and analysed for green fluorescence using a FL-1 channel flow cytometer.

Fig. 11. Flow cytometric analysis of the apoptotic and necrotic cells induced by complexes **1-6** and cisplatin. HeLa cells were stained with Annexin V-FITC and PI after 48 hours of incubation with IC_{50} concentrations of the metal complexes. (LL: live; LR: early apoptotic; UR: late apoptotic; UL: necrotic).

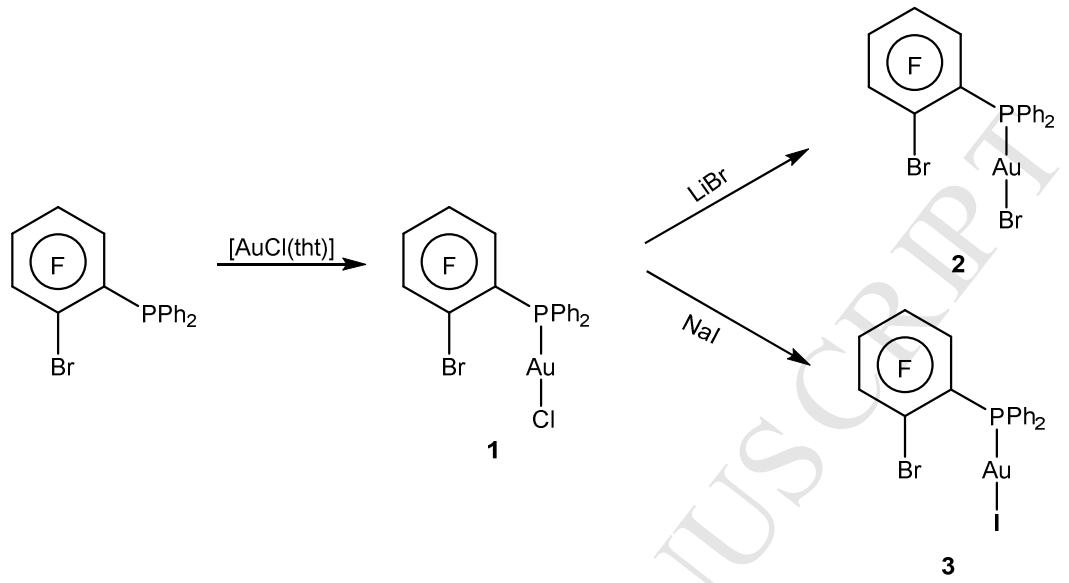

Scheme 1. Synthesis of neutral gold(I) complexes (**1-3**)

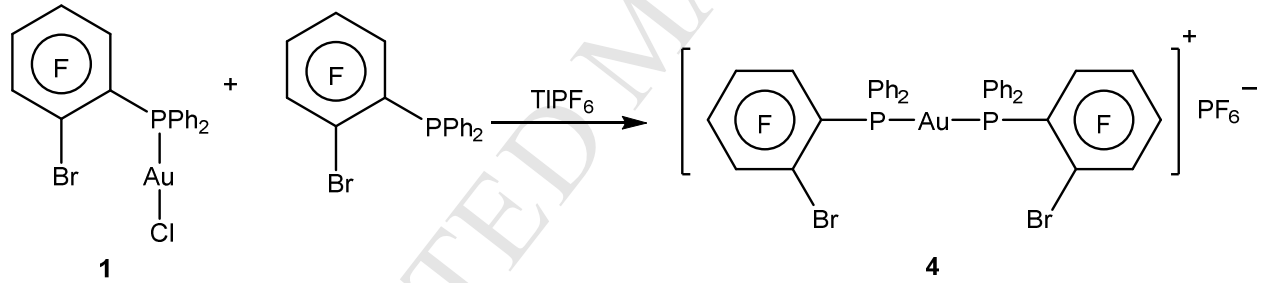

Scheme 2. Synthesis of a cationic gold(I) complex (**4**)

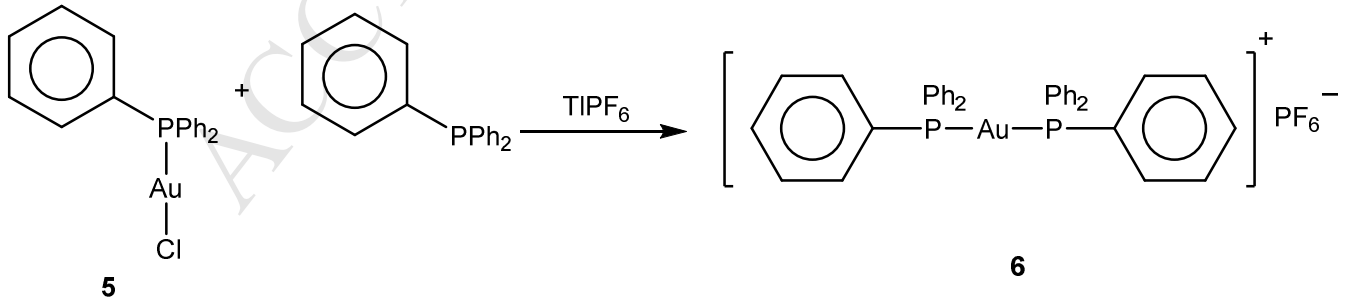

Scheme 3. Synthesis of a cationic gold(I) complex (**6**)

Table 1. Selected bond distances (Å) and angles (º) in complexes **1-4.**

	1, X = Cl(1)	**2**, X = Br(2)	**3**, X = I(1)		**4**
Au(1)–P(1)	2.2307(11)	2.2407(10)	2.2468(8)	Au(1)–P(1)	2.2976(7)
Au(1)–X	2.2817(11)	2.3975(5)	2.5413(3)	Au(1)–P(1*)	2.2976(7)
X–Au(1)–P(1)	176.98(2)	178.07(3)	179.68(2)	P(1)–Au(1)–P(1*)	180.0

Table 2. IC_{50} values (μM)* of the gold phosphine complexes against selected human cancer cell lines and normal cell line (Hek-293T).

Complex	**PC3**	**U87MG**	**HeLa**	**HT1080**	**SKOV-3**	**Hek-293T**
1	12.2±1.66	8.1±0.83	15.1±2.4	6.51±1.1	13.1±2.52	16.8±3.81
2	22.5±1.94	7.31±0.72	13.8±1.16	7.32±0.85	18.3±3.42	18.9±2.82
3	1.96±0.36	2.62±0.24	8.7±1.23	6.03±0.51	10.3±2.31	12.3±0.81
4	3.14±0.73	2.1 ±0.56	1.9±0.68	3.11±0.27	2.83±0.24	5.85±0.63
5	4.53±0.41	5.57±0.21	2.57±0.15	4.66±0.63	8.93±1.23	1.98±0.22
6	4.01±0.46	3.78±0.42	1.23±0.11	3.57±0.37	6.12±0.85	6.83±0.92
Cisplatin	6.31±0.23	8.22±0.81	3.25±0.28	0.63±0.12	1.57±0.36	4.78±0.35

* IC_{50} values are the concentrations that cause 50% inhibition of cancer cell growth. Data represent the mean values ± standard deviation of three independent experiments performed in triplicate.

Table 3. Thioredoxin reductase (TrxR) and glutathione reductase (GR) inhibition activity (EC_{50}, μM)* of the gold phosphine complexes **1–6**.

Complex	TrxR	GR	Selectivity GR/TrxR (x fold)
1	0.15±0.05	2.65±0.16	17.6
2	0.27±0.11	1.93±0.24	7.1
3	0.11±0.03	6.9±1.12	62.2
4	2.6±0.31	15.6±0.36	6.0
5	0.28±0.09	1.5±0.07	5.3
6	3.5±0.27	10.7±0.54	3

* The concentration of the metal complex required for 50% inhibition of enzyme activity. Data represents the mean of triplicate runs of three independent experiments.

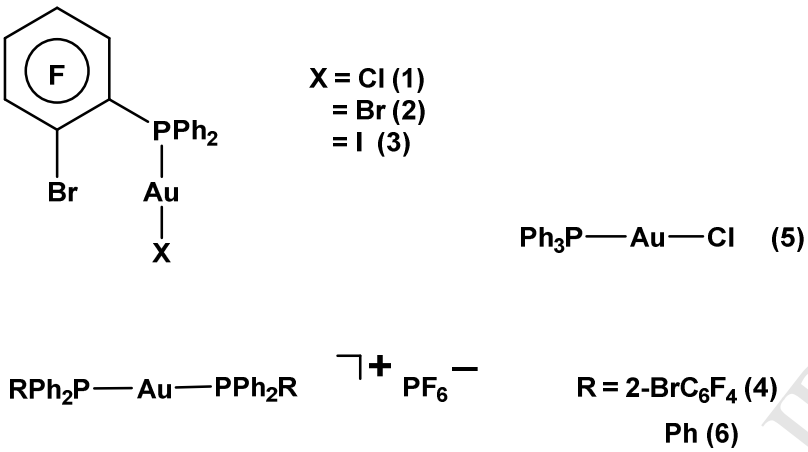

Fig. 1. Structures of the gold(I) phosphine complexes used in this investigation.

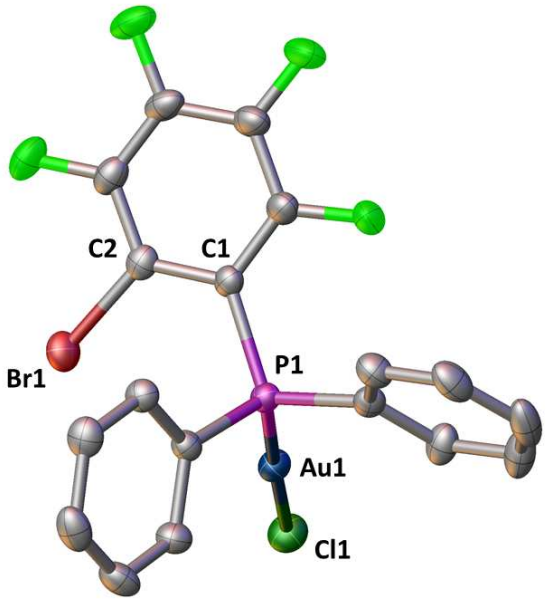

Fig. 2. Molecular structure of [AuCl(2-$BrC_6F_4PPh_2$)] (**1**). Ellipsoids show 50% probability levels and hydrogen atoms have been omitted for clarity. Only one molecule in the asymmetric unit is shown.

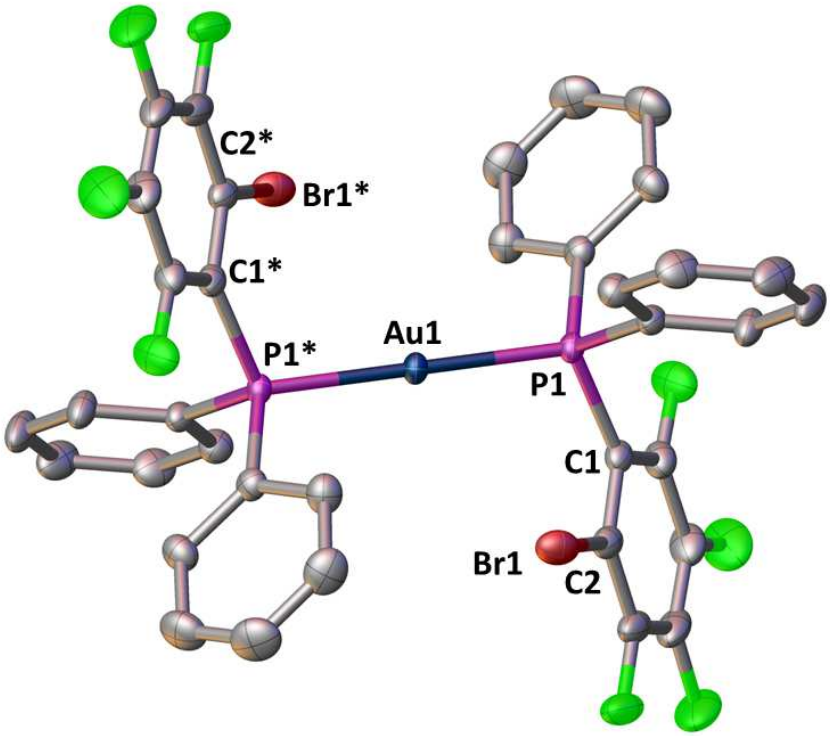

Fig. 3. Molecular structure of the cation in $[Au(2\text{-}BrC_6F_4PPh_2)_2]PF_6$ (**4**). Ellipsoids show 50% probability levels. Hydrogen atoms and PF_6 counter ion have been omitted for clarity. Only one molecule in the asymmetric unit is shown.

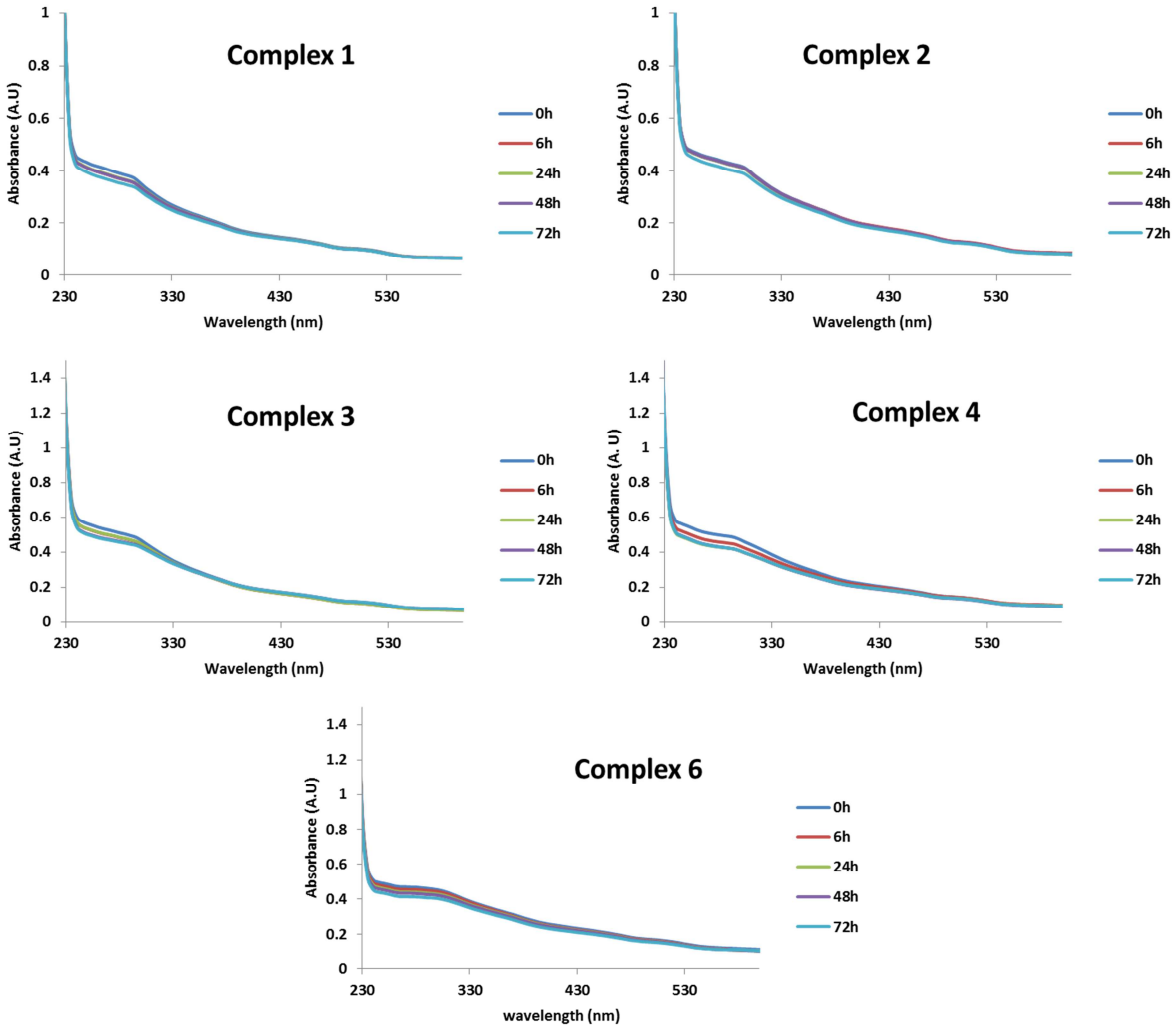

Fig. 4. UV-Vis absorption spectra of the gold(I) complexes (25 µM) in sodium phosphate buffer (50 mM, pH 7.4) over 72h.

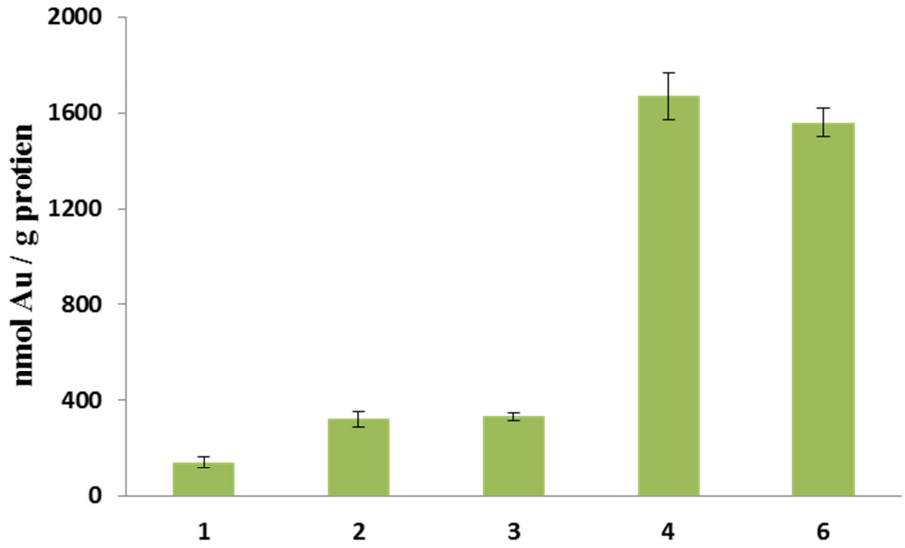

Fig. 5. The amount of gold taken up by cervical cancer cells (HeLa) after exposure to IC_{50} concentrations of gold complexes for 24 h.

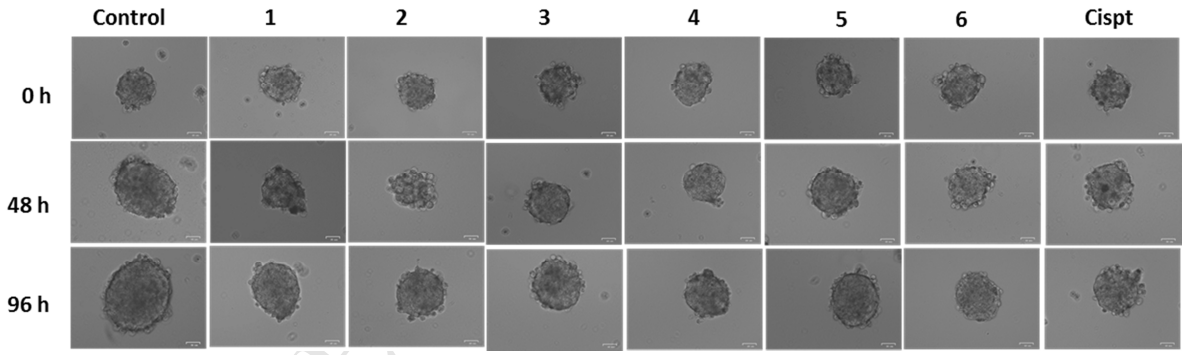

Fig. 6. Effect of complexes **1-6** and cisplatin on HeLa spheroid formation. HeLa cells were grown in ultra-low attachment plates and treated with IC_{50} concentrations of the metal complexes for the spheroid assay. After 48 h and 96 h, the spheroids were photographed.

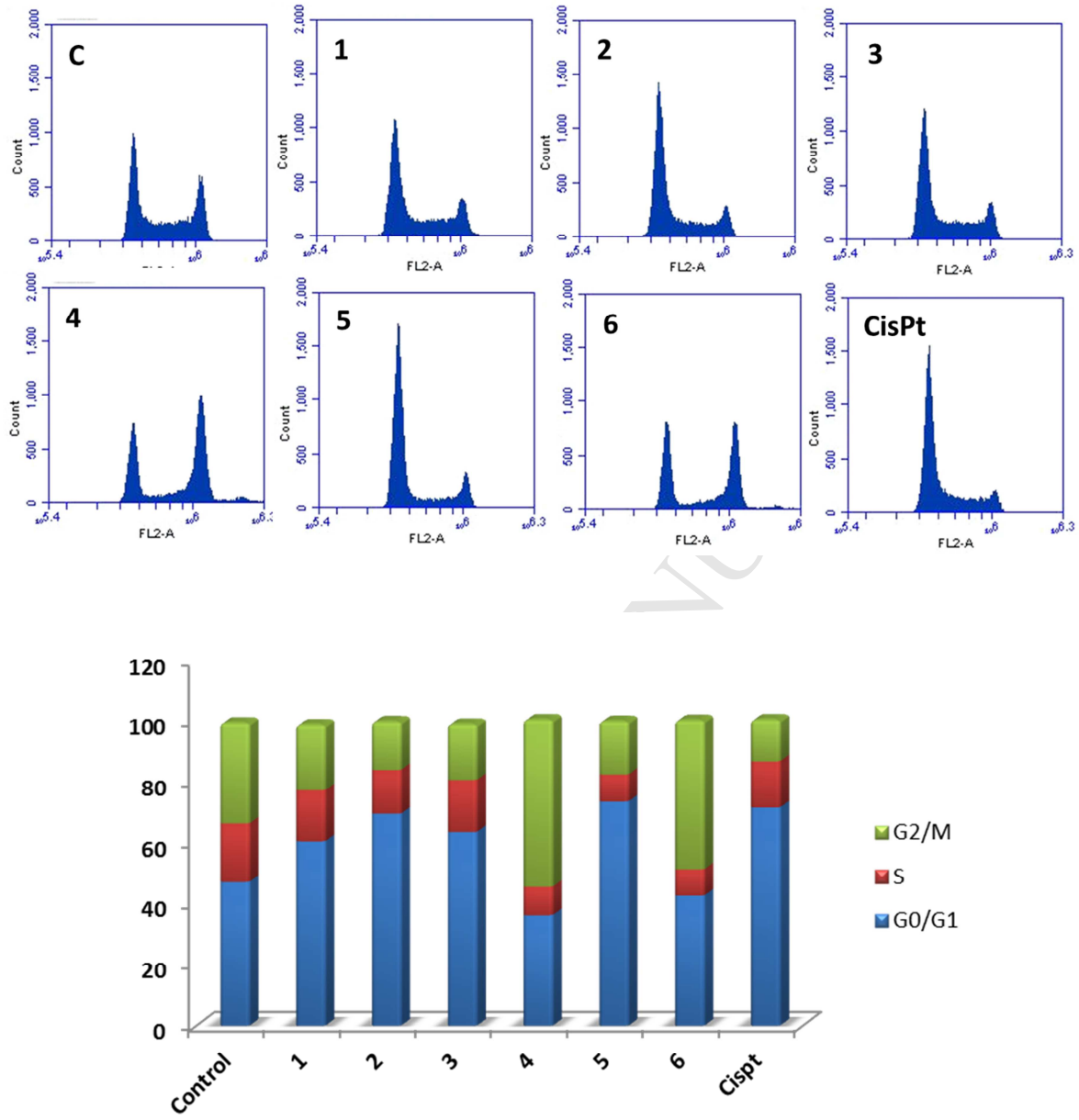

Fig. 7. Cell cycle distribution of HeLa cells after treatment with the gold complexes **1-6** and cisplatin for 48 h. The percentage of cells in each phase was analysed using BDC6 accuri software.

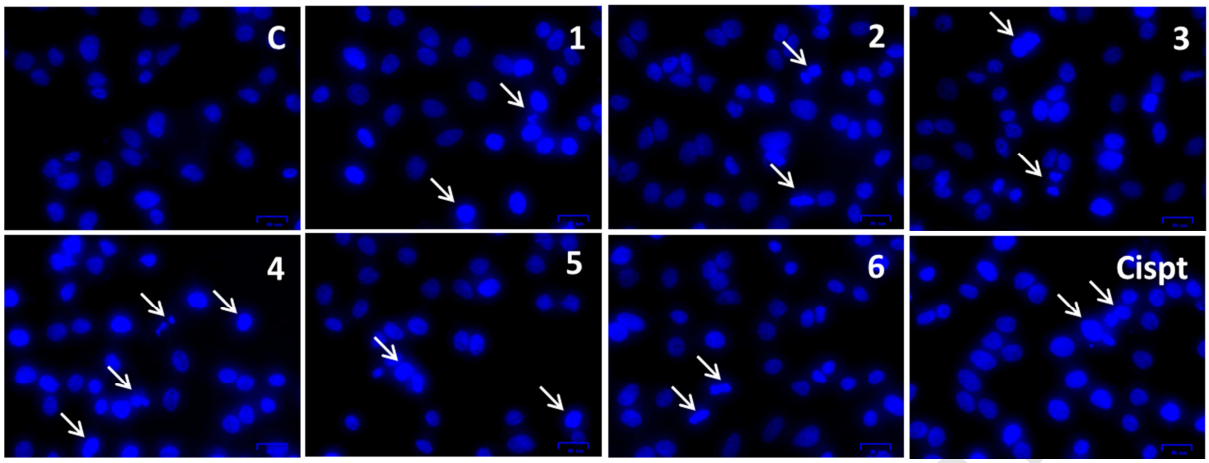

Fig. 8. Apoptosis in HeLa cells induced by complexes **1-6** and cisplatin, observed using Hoechst 33242 staining. HeLa cells were incubated with IC_{50} concentrations of the complexes for 48 h. The morphological changes of cell apoptosis such as condensation of chromatin and nuclear fragmentations were observed by fluorescence microscopy after staining with Hoechst 33242.

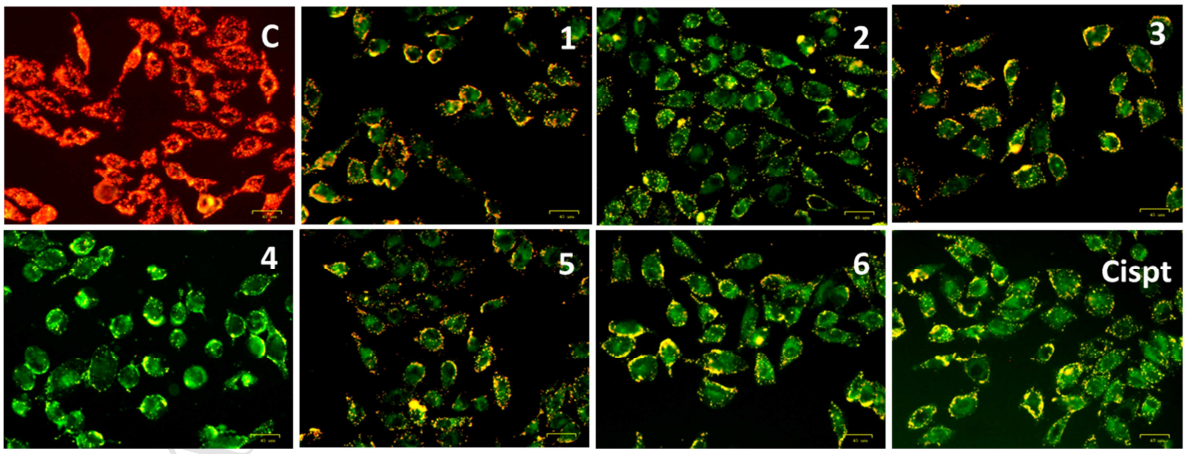

Fig. 9. Fluorescence microscopic images of mitochondrial membrane integrity disruption in HeLa cells induced by treatment with complexes **1-6**. HeLa cells were treated with IC_{50} concentrations of the metal complexes for 48 h before staining with JC-1 and were imaged by fluorescence microscopy.

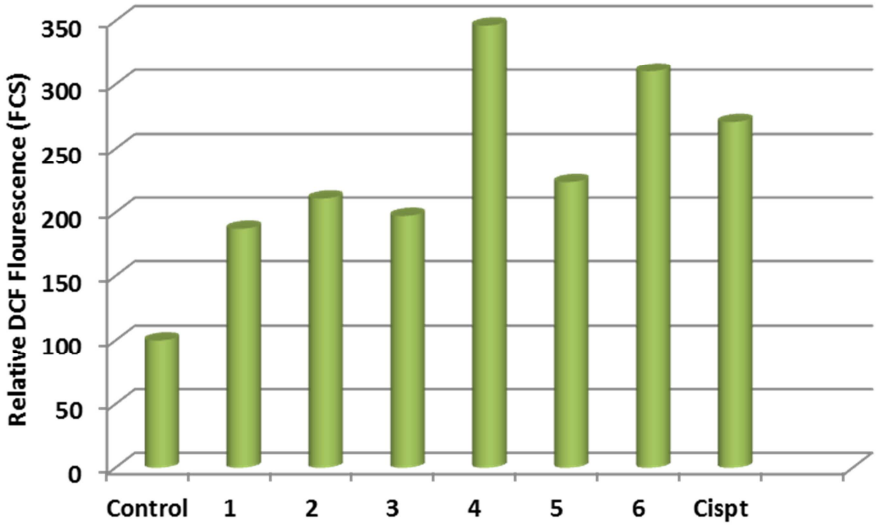

Fig. 10. Metal complex induced production of intracellular ROS in HeLa cancer cells. Cells were treated with IC_{50} concentrations of the metal complexes for 48 h, stained with 10 μM DCF-DA and analysed for green fluorescence using a FL-1 channel flow cytometer.

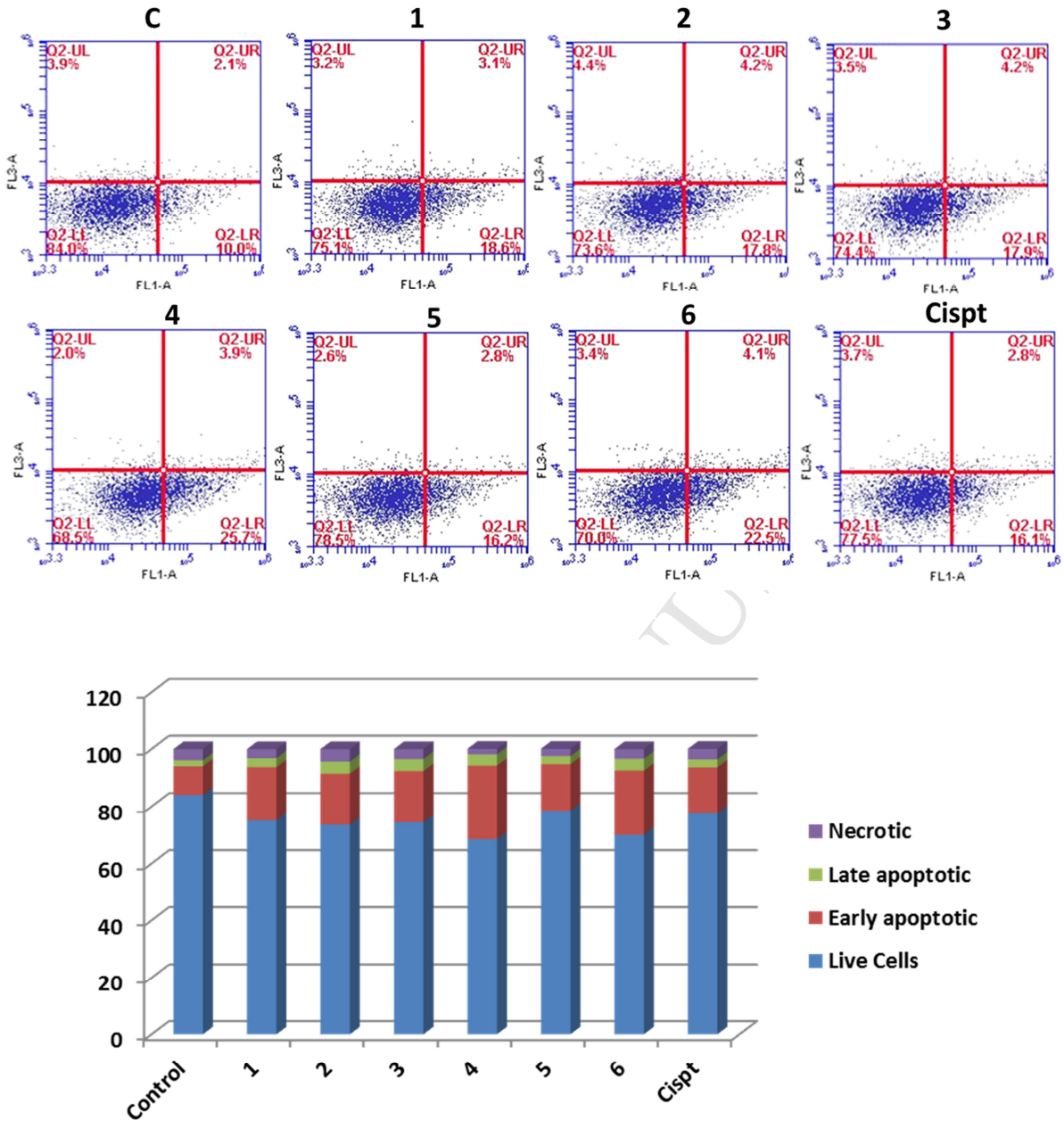

Fig. 11. Flow cytometric analysis of the apoptotic and necrotic cells induced by complexes **1-6** and cisplatin. HeLa cells were stained with Annexin V-FITC and PI after 48 hours of incubation with IC_{50} concentrations of the metal complexes. (LL: live; LR: early apoptotic; UR: late apoptotic; UL: necrotic).

- Gold(I) phosphine complexes containing 2-Br-$C_6F_4PPh_2$ ligand were synthesised.
- The cationic metal complexes **4** and **6** showed excellent anti-proliferative activities.
- The metal complexes exhibited inhibition of solid tumor growth in 3D multicellular spheroids of HeLa cells.
- The metal complexes induces apoptosis through cell cycle arrest and mitochondria mediated damage.